Paper

Int'l J. of Aeronautical & Space Sci. 16(2), 137–147 (2015)
DOI: http://dx.doi.org/10.5139/IJASS.2015.16.2.137

IJASS
International Journal of Aeronautical and Space Sciences

Compromise Optimal Design using Control-based Analysis of Hypersonic Vehicles

Yanbin Liu* and Hua bing**

College of Astronautics, Nanjing University of Aeronautics and Astronautics, Nanjing 210016, China

Abstract

Hypersonic vehicles exhibit distinct dynamic and static characteristics, such as unstable dynamics, strict altitude angle limitation, large control bandwidth, and unconventional system sensitivity. In this study, compromise relations between the dynamic features and static performances for hypersonic vehicles are investigated. A compromise optimal design for hypersonic vehicles is discussed. A parametric model for analyzing the dynamic and static characteristics is established, and then the optimal performance indices are provided according to the different design goals. A compromise optimization method to balance the dynamic and static characteristics is also discussed. The feasibility of this method for hypersonic vehicles is demonstrated.

Key words: Hypersonic Vehicles, Compromise Optimal Design, Dynamic Characteristics, Flight Stability, Parametric Model.

1. Introduction

Critical design issues, such as the aero-thermo-elastic-propulsion coupling relations and scramjet propulsive theories, are extensively investigated with the advancement of hypersonic technologies. Research has aimed at developing hypersonic transportation systems for a reliable and affordable transport to space and global reach vehicles [1]. Extensive studies have been focused on the control-orienting analysis and control integrated design for hypersonic vehicles [2]. These vehicles should incorporate control-centric considerations associated with strong relations between aerodynamics, propulsion, structure, and controls during the conceptual stages of vehicle design. Thus, several control-relevant problems, such as the input/output coupling, unstable/non-minimum phase, and uncertain dynamic effects, should be carefully explored to obtain the overall design [3]. Multidisciplinary design optimization using the control-centric idea should be introduced to the design of waverider configuration to improve the general performance of hypersonic vehicles.

Compared with conventional vehicles, hypersonic vehicles exhibit unique wave-riding features and operate with high dynamic pressure in uncertain and unknown environments [4]. In addition to the dynamic complexity and unexpected coupling between the airframe and the propulsion system, physical limitations on the control inputs presents numerous challenges for the implementation of continuous control throughout a large flight envelope. Therefore, establishing a high-fidelity model and designing an adaptive controller for hypersonic vehicles are critical to realize the anticipated tasks. A high-fidelity model of the longitudinal dynamics for an air-breathing hypersonic vehicle was developed [5], from which a control-oriented model was built with curve-fitted approximations [6] to provide the control design object. In addition, a wing/pivot system model [7], a nonlinear ten-degree-of-freedom dynamics model [8], and a three-dimensional flexible model [9] were provided in the design of flight control systems as well as the evaluation of flight stability. Based on these established models, a reference command tracking control law was presented by using the H∞ method to achieve excellent tracking performance of hypersonic vehicles in [10]. Moreover, a linear parameter-varying switching tracking control scheme was proposed

* Associate Professor, Corresponding author: nuaa_liuyanbin@139.com
** Associate Researcher

Received: March 16, 2015 Revised: May 24, 2015 Accepted: June 5, 2015

http://ijass.org pISSN: 2093-274x eISSN: 2093-2480

[11] for a hypersonic vehicle model to satisfy a specified performance criterion. In addition, a novel finite time control method was used for the longitudinal model of the hypersonic vehicle to optimize operation [12]. Several advanced control approaches were adopted to design the robust adaptive controller for hypersonic vehicles. These techniques include high-order dynamic sliding mode control method [13], neural control mean [14], and adaptive back-stepping control strategies [15]. Establishing a model of the hypersonic vehicle is important for designing a feasible controller, thus ensuring the wavering stability and completing the command track.

However, a nonlinear model of a hypersonic vehicle restricts the control design space, and thus the control specifications are unable to meet the anticipated demands under certain flight conditions. Consequently, compromise between the nonlinear model and control qualities for hypersonic vehicles should be investigated. A comprehensive analysis of the dynamic and static characteristics is beneficial in coordinating the relations associated with the inherent model dynamics and expected close-loop control performances. In this aspect, the sensitivity of flight dynamics was analyzed for hypersonic vehicles to understand the design tradeoffs required and contribute to the control design [16]. In addition, the influence on design parameters combined with various limit-of-performance metrics was considered for hypersonic vehicles to explore the varying trends for model dynamics matched with additional control constraints [17]. Furthermore, fundamental limitations were studied for the model dynamics and closed loop control performances of hypersonic vehicles to complete further control-relevant design [18]. Hence, multidisciplinary optimization approaches [19] should be introduced to the design of a hypersonic vehicle to achieve coordinating maneuver concerning the nonlinear model and control performance.

This study investigates compromise optimal design methods by integrating dynamic and static characteristics of hypersonic vehicles. Several aspects of this issue are considered. First, the waverider model is established using multidisciplinary estimation methods. Second, the dynamics feature is analyzed, and control-based performance indices are constructed. Third, an optimization technique is selected to iterate the provided performance functions according to the viewpoint of the integration of dynamic and static characteristics. Lastly, the feasibility of the presented design methods is verified for a typical waverider configuration. The design goal of the compromise optimization is simultaneously realized for hypersonic vehicles.

2. Dynamic Modeling Using Multidisciplinary Knowledge of Hypersonic Vehicles

Hypersonic vehicles adopt waverider configuration to acquire high lift-drag ratio and improved propulsive efficiency. However, such shape will affect flight stability; for example, any change in the flight altitude leads to thrust alteration because of the strong aerodynamic-propulsion coupling dynamics. A basic waverider structure is applied in this study to reflect this relation (Fig.1).

Figure 1 shows a typical two-dimensional waverider configuration, and the lower surface of the forebody is considered as a curve surface where the airflow is continually compressed before entering the propulsive systems. In turn,

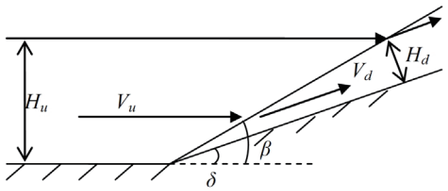

Fig.2. Schematic diagram of concave surface

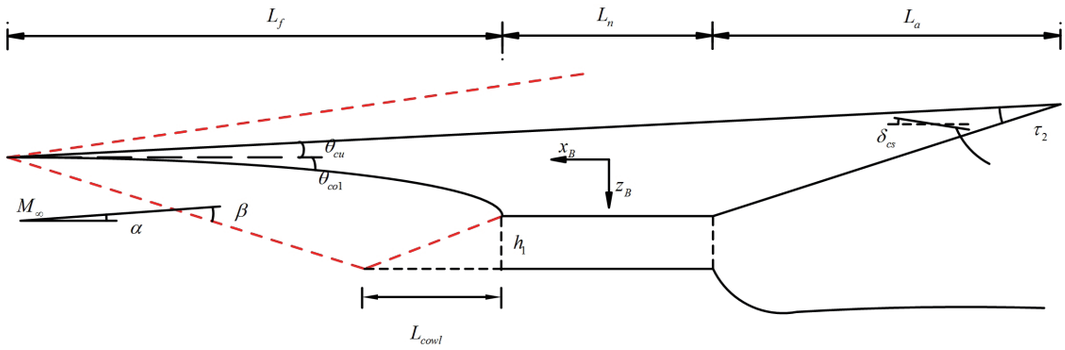

Fig.1. Basic shapes of hypersonic waverider

DOI: http://dx.doi.org/10.5139/IJASS.2015.16.2.137

the airstream encounters the concave surface, shown in Fig. 2.

The oblique shock wave principle is used to compute the according pressure given in [20]

$$\begin{cases} \tan(\delta) = \dfrac{2\cot\beta(M_u^2\sin^2\beta - 1)}{M_u^2(\gamma_c + 1 - 2\sin^2\beta) + 2} \\ \dfrac{P_d}{P_u} = 1 + \dfrac{2\gamma_c}{\gamma_c + 1}(M_u^2\sin^2\beta - 1) \end{cases} \tag{1}$$

where δ denotes the airflow turning angle; β is the shock wave angle; P_u and M_u indicate respectively the pressure and Mach with regard to the upstream airflow; P_d represents the pressure of the condensed airflow; γ_c is the specific heat ratio. Alternatively, the airflow enters the convex surface, displayed in Fig. 3.

In this case, the expansion wave theory is applied to estimate the surface pressure, and it is expressed by [5, 21]

$$\begin{cases} \nu(M_u) = \sqrt{\dfrac{\gamma_c+1}{\gamma_c-1}}\tan^{-1}\left(\sqrt{\dfrac{\gamma_c+1}{\gamma_c-1}(M_u^2-1)}\right) - \tan^{-1}\left(\sqrt{M_u^2-1}\right) \\ \nu(M_d) = \nu(M_u) + \theta_d - \theta_u \\ \dfrac{P_d}{P_u} = \left[\dfrac{1+\dfrac{\gamma_c-1}{2}M_u^2}{1+\dfrac{\gamma_c-1}{2}M_d^2}\right]^{\frac{\gamma_c}{\gamma_c-1}} \end{cases} \tag{2}$$

where θ_d and θ_u are respectively the angles between the compression surfaces and level surface, shown in Fig. 3. When the pressures on each surface are gotten based on Equations (1) and (2), the aerodynamic forces are estimated by [5]

$$\begin{cases} L = F_x\sin\alpha - F_z\cos\alpha \\ D = -F_x\cos\alpha - F_z\sin\alpha \end{cases} \tag{3}$$

where

$$\begin{cases} F_x = F_{x,f} + F_{x,u} + F_{x,n} + F_{x,t} + F_{x,a} + F_{x,e} \\ F_z = F_{z,f} + F_{z,u} + F_{z,n} + F_{z,t} + F_{z,a} + F_{z,e} \end{cases} \tag{4}$$

where the subscripts f and u are respectively the forebody and upper surface; the subscripts n and t denote the undersurface and airflow transition layer, respectively; the subscripts a and e represent respectively the afterbody and elevator deflection; α indicates the angle of attack. In addition to these aerodynamic forces, the propulsive force T is calculated by [22]

$$T = \dot{m}_a\left(1+\phi f_{st}\right)V_o - \dot{m}_a V_\infty + P_o A_o - P_\infty A_i \tag{5}$$

where ϕ and f_{st} denote the equivalence ratio and stoichiometric fuel–air ratio, respectively; V_∞ and P_∞ are the freestream speed and pressure, respectively. V_o and P_o represent the exhaust exit speed and airflow pressure respectively which are determined by the Rayleigh flow relations and entropy principle in [23]; A_i and A_o are the inlet area and exit area, respectively; $\dot{m}_a$ indicates the air flow rate which has the significant influence on the propulsive efficiency. For instance, the two compression section of the forebody is show in Fig. 4.

Based on the geometric relationships in Fig. 4, the equivalent airflow height H_∞ is gotten as follows:

$$\begin{cases} H_\infty = \dfrac{|EP|\sin\beta_{s2}\sin\beta_{s1}}{\sin\left(\beta_{s2}+\theta_{co1}-\theta_{co2}\right)\sin\left(\beta_{s1}-\theta_{co1}-\alpha\right)} \\ |EP| = \left(H_1 - L_{cowl}\tan\delta_{cowl}\right)\cos\theta_{co2} + L_{cowl}\sin\theta_{co2} \end{cases} \tag{6}$$

where L_{cowl} and δ_{cowl} are respectively the length and turning angle of the inlet cowl depicted in Figs. 1 and 4; θ_{co1} and θ_{co2}

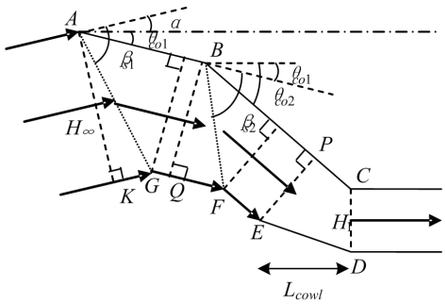

Fig.4. Schematic diagram of two-stage forebody compression section

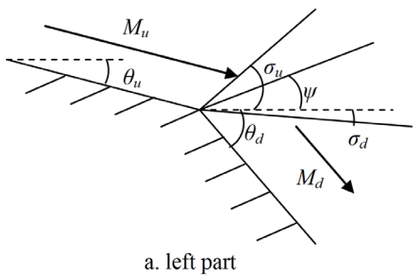

a. left part

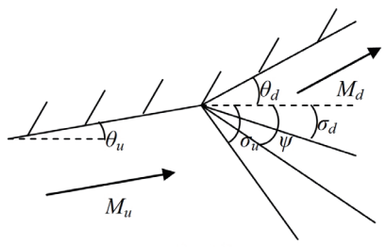

b. right part

Fig. 3. Schematic diagram of convex surface

denote the first compression angle and second compression angle, respectively; H_1 indicate the inlet height. Afterwards, the air flow rate is estimated by [24]

$$\dot{m}_a = P_\infty M_\infty \sqrt{\frac{\gamma_c}{RT_\infty}} H_\infty W_\infty \tag{7}$$

where R denotes the universal constant; T_∞ is the temperature of the free flow; W_∞ indicates the width of the inlet. Once these aerodynamic forces and thrust are known, the nonlinear model of hypersonic vehicle is demonstrated as follows: [4, 25]

$$\begin{cases} \dot{v} = \left[\dfrac{T\cos\alpha - D}{m}\right] - g\sin(\theta-\alpha) \\ \dot{\alpha} = -\left[\dfrac{L + T\sin\alpha}{mv}\right] + q + \dfrac{g}{v}\cos(\theta-\alpha) \\ \dot{q} = \dfrac{M_y}{I_y} \\ \dot{h} = v\sin(\theta-\alpha) \\ \dot{\theta} = q \end{cases} \tag{8}$$

where h and v denote the flight altitude and velocity, respectively; θ and q represent respectively the pitch angle and its change rate; M_y and I_y indicate the pitch moment and moment of inertia, respectively; m and g are respectively the vehicle mass and gravitational constant.

Based on Equation (8), the elevator deflection angle δ_e and equivalence ratio ϕ are selected as the control input vector U, whereas v and h are considered as the control output vector Y. Thus, Equations (3), (5), and (8) constitute the complete nonlinear model of a hypersonic vehicle. Beyond this, for the given flight condition, the trim states, namely, α_b, δ_{eb}, and ϕ_b can be solved according to these forces, and then the linear model is constructed as follows.

$$\begin{cases} \Delta\dot{X} = A(h,v)\Delta X + B(h,v)\Delta U \\ \Delta Y = C(h,v)\Delta X + D(h,v)\Delta U \end{cases} \tag{9}$$

where $\Delta X \triangleq [\Delta v, \Delta\alpha, \Delta q, \Delta h, \Delta\theta]^T$. Based on Equation (9), the transfer function of the linear model is obtained as

$$G(s) = C(sI - A)^{-1} B + D \tag{10}$$

According to Equations (9) and (10), the following works are performed to analyze the dynamic and static characteristics of a hypersonic vehicle according to control orienting demands. Moreover, if this model can be perceived as the control object, some classic and modern control methods can be applied to design the robust flight control system for hypersonic vehicles [26].

3. Performance indices and compromise optimization for hypersonic vehicles

First, the nonlinear model in Equation (8) is considered. For the given flight Mach and altitude, the trim values are solved as follows:

$$\begin{cases} T(\alpha_b, \delta_{eb}, \phi_b)\cos\alpha_b - D(\alpha_b, \delta_{eb}, \phi_b) = 0 \\ L(\alpha_b, \delta_{eb}, \phi_b) + T(\alpha_b, \delta_{eb}, \phi_b)\sin\alpha_b - mg = 0 \\ M_y(\alpha_b, \delta_{eb}, \phi_b) = 0 \end{cases} \tag{11}$$

As soon as the trim parameters α_b, δ_{eb}, and ϕ_b are obtained, the linear model is acquired accordingly. However, α_b, δ_{eb}, and ϕ_b may not satisfy the design requirements for the given flight condition because input saturation and altitude angle limitation are considered. Therefore, suitable adjustment at the flight point is necessary to identify the feasible flight region. In particular, the equation of pitching moment is very important for analyzing the trim state, because the pitching moment is affected by force distribution, elevator area and position, propulsive direction, mass change, and so on. Therefore, the matching changes in the angle of attack and elevator deflection angle can regulate the pitching moment such that the balance relation is achieved for the hypersonic vehicle.

However, adjusting the angle of attack and elevator deflection angle is limited for a hypersonic flight. Specially, the trim angle of attack should be constrained within the certain range in which the scramjet can function well. In turn, the trim elevator deflection angle and propulsive coefficient should escape the input saturation to guarantee larger control authority [27]. Based on these features, the static feature specification is considered as follows:

$$J_s(Ma_0, h_0, S_b) = \min[C_\alpha |\alpha_b - \alpha_0| + C_\delta |\delta_b| + C_\phi |\phi_b|] \tag{12}$$

where α_0 is the expected angle of attack. C_α, C_δ, and C_ϕ denote the selected index coefficients, and S_b=[α_b, δ_b, ϕ_b]. Equation (12) shows the coordinating optimization relations in relation to the trim values. Beyond this, the dynamic characteristics should be further considered in this paper. Thus, the transfer function between the flight path angle and elevator deflection angle is emphatically discussed, which was explored in Ref. [27]:

$$\frac{\Delta\gamma(s)}{\Delta\delta_e(s)} = \frac{c_\gamma(s+z_{\gamma 1})(s+z_{\gamma 2})(s+z_{\gamma 3})}{(s^2 + 2\xi_p\omega_p s + \omega_p^2)(s+z_{sp1})(s+z_{sp2})} \tag{13}$$

where ω_p and ξ_p are the frequency and damp of the long-term mode, respectively. Z_{sp1} and Z_{sp2} denote the poles of the short-term mode. Z_{r1}, Z_{r2} and Z_{r3} indicate the according zeros.

DOI: http://dx.doi.org/10.5139/IJASS.2015.16.2.137

c_r represents the gain of this transfer function. For Equation (13), a right-half plane zero caused by the appearance of the negative lift exists as the elevator deflects trailing edge up. Without loss of generality, Z_{r3} is selected as this zero, given by [28], as follows:

$$z_{\gamma 3} = \sqrt{M_\alpha - \frac{M_{\delta_e}}{z_{\delta_e}} z_\alpha} \tag{14}$$

where M_α and M_{δ_e} are the derivatives of the pitch moment along with the angle of attack and elevator deflection angle, respectively. Z_α and Z_{δ_e} represent the derivatives of the lift force along with the angle of attack and elevator deflection angle, respectively.

The existence of this non-minimum phase zero constrains the available upper boundary on the system bandwidth of the close-loop control system [28]. However, one of the poles in the short-term mode remains in the right-half plane because applying the slender waverider structure ensures that the instantaneous center-of-rotation is always in front of the center-of-mass. Consequently, the dynamic model of a hypersonic vehicle has an unstable pole, which constrains a lower bound on the control bandwidth, because the frequency of the close-loop control system should be greater than the frequency of the unstable pole [28]. Accordingly, the optimal design goal of dynamic characteristics reflects that the frequency ω_{sp} of the unstable pole maintains a small value, and the right-half plane zero is simultaneously far from the imaginary axis. Thus, the dynamic feature specification is designed as follows:

$$J_d(Ma_0, h_0, W_s) = \min\left[c_{sp} \left|\omega_{sp}\right| + \frac{c_{\gamma 3}}{\left|\omega_{\gamma 3}\right|} \right] \tag{15}$$

where c_{sp} and c_{r3} denote the selected index coefficients, and W_s=[ω_{sp}, ω_{r3}]. Nevertheless, the performance index that only uses Equation (12) or (15) is not sufficient to guarantee the satisfactory overall performance of a hypersonic vehicle. Hence, the compromise design for these features is necessary. The following optimization index is presented.

$$\begin{aligned} J(Ma_0, h_0, S_b, W_s) &= J_s(Ma_0, h_0, S_b) + J_d(Ma_0, h_0, W_s) \\ &= \min\left[C_\alpha \left|\alpha_b - \alpha_0\right| + C_\delta \left|\delta_b\right| + C_\phi \left|\phi_b\right| + c_{sp} \left|\omega_{sp}\right| + \frac{c_{\gamma 3}}{\left|\omega_{\gamma 3}\right|} \right] \end{aligned} \tag{16}$$

Equation (16) can achieve the compromise optimal design results, leading to the trade-off relations among the waverider configuration, control efficiency, and flight condition. Furthermore, optimizing the flight condition for the given waverider configuration is investigated, and the flight Mach is regarded as the optimal variable corresponding to the given flight height. Correspondingly, the compromise optimization is expressed as follows:

$$Ma_0 = \begin{cases} \min & J(h_0, S_b, W_s) \\ \text{s.t.} & Ma_{\min} \le Ma \le Ma_{\max} \end{cases} \tag{17}$$

For Equation (17), the Lagrange function is introduced as follows:

$$L_{Ma} = J(h_0, S_b, W_s) - \lambda_{Ma} Ma \tag{18}$$

where λ_{Ma} is the Lagrange function coefficient. The following performance function is built as follows:

$$Ma_0 = \min \Gamma = \sum_{S_b} \left(\frac{\partial J}{\partial S_b} \right)^2 + \sum_{W_s} \left(\frac{\partial J}{\partial W_s} \right)^2 + \lambda_{Ma} Ma^2 \tag{19}$$

By using the steepest descent method, the iterative step in the compromise optimal design is given as follows:

$$Ma^{(k+1)} = Ma^{(k)} - \lambda_{Ma} \nabla \Gamma \left(Ma^{(k)} \right) \tag{20}$$

where $-\nabla\Gamma$ represents the negative gradient direction. According to Equation (20), once the absolute gradient of Γ is smaller than the expected value, the iteration stops. Accordingly, the optimal flight velocity is acquired such that the compromise design between static features and dynamic characteristics can be realized for the hypersonic vehicle.

4. Illustrative Example

The waverider configuration in Fig. 1 is adopted to verify the effectiveness of the presented methods. The geometric parameters of the hypersonic vehicle are provided in Table 1 [5]. Several shape parameters are slightly different from those in Ref. [5] because the waverider configuration in Fig. 1 considers the forebody as the two-stage compression section for improving propulsive efficiency.

Once these model parameters are introduced to Fig. 1, the aerodynamic forces and thrust can be obtained using the estimating theories in Section 2. Based on Equation (11), the trim values are solved on the given flight condition. Furthermore, the static feature specification in Equation (12) is considered. In this case, the flight altitude range is selected from 28 km to 30 km, and the expected angle of attack is limited to 1° at the same time. The resulting curves are provided in Figs. 5 and 6.

By using Equation (12), the maximum value of the optimal flight Mach is calculated as 7.51 with the height of 30 km (Figs. 5 and 6). In this case, the right-half plane pole and

zero are 3.04 and 6.29, respectively, whereas the trim angle of attack, elevator deflection angle, and equivalence ratio are 1.09°, 15.41°, and 0.6, respectively. For comparison, the dynamic feature specification in Equation (15) is considered, and simulation results are shown in Figs. 7 and 8.

By using Equation (15), the maximum value of the optimal flight Mach is calculated as 9.22 with the height of 30 km (Figs. 7 and 8). This result demonstrates that the optimal value using the dynamic characteristic specification is evidently distinct from that using the static feature specification. More importantly, the trim angle of attack is far from the anticipated value. These results imply the presence of design contradiction between dynamic characteristics and static features. Consequently, the compromise design should be fully considered for hypersonic vehicles. Accordingly, the performance index in Equation (16) is adopted in the simulation, and the resulting curves are displayed in Figs. 9 and 10.

The optimal results can meet compromise design demands. The compromise design can synthesize static features and dynamic characteristics such that the generalized performance is improved accordingly

Table 1. Geometric parameters of hypersonic vehicle

Parameter names	Symbols	Values
The length of the forebody	L_f	14.33m
The length of the afterbody	L_a	10.06m
The engine length	L_n	6.09m
The forebody turn angle	θ_{co1}	3°
The afterbody turn angle	τ_2	14.34°
The inlet height	h_1	1m
The inlet width	W_∞	0.3048m
The length of the inlet cowl	L_{cowl}	4m
The elevator area	$S_{\delta e}$	1.58m^2
The vehicle mass	m	2000kg
The moment of inertia	I_y	5×10^5 kg*m^2
The center position of gravity	C_g	(-16.8m,0)

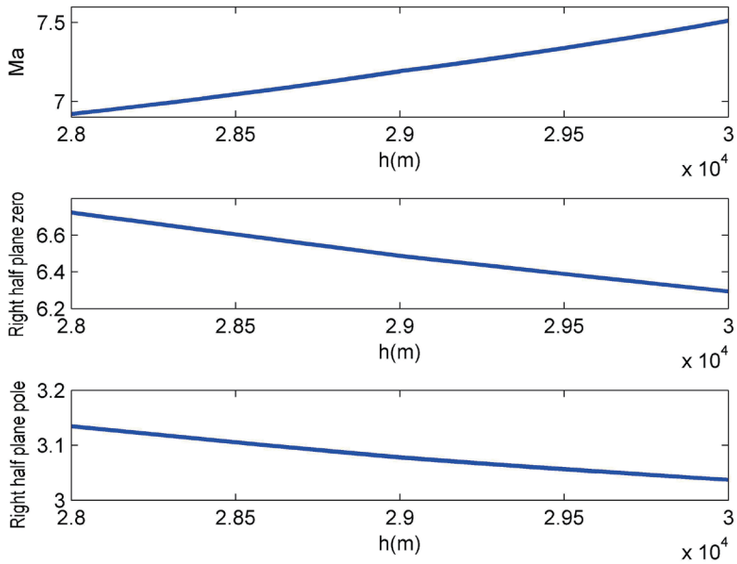

Fig.5. Optimal results in consideration of static feature specification

DOI: http://dx.doi.org/10.5139/IJASS.2015.16.2.137

compared with the single performance index. Moreover, the different specifications in Equations (12), (15), and (16) are considered, and the comparative results are listed in Table 2.

According to Table 2, the right-half plane zero will be closer to the imaginary axis when the static feature specification in Equation (12) is used compared with that with the use of the integrated index in Equation (16). By contrast, the index in Equation (15) results in the deviation of the trim angle of attack from 1°, even reaching an unexpected negative value. These results demonstrate that the compromise specification in Equation (16) is better than that in Equations (12) and (15) because the optimized flight conditions are acquired by applying the compromise optimal design for hypersonic vehicles. In particular, aerodynamic forces estimated using Equations (1) and (2) yield some errors because of the calorically perfect gas assumption. However, the main inherent features can be fully reflected using the optimal design process associated with the compromise

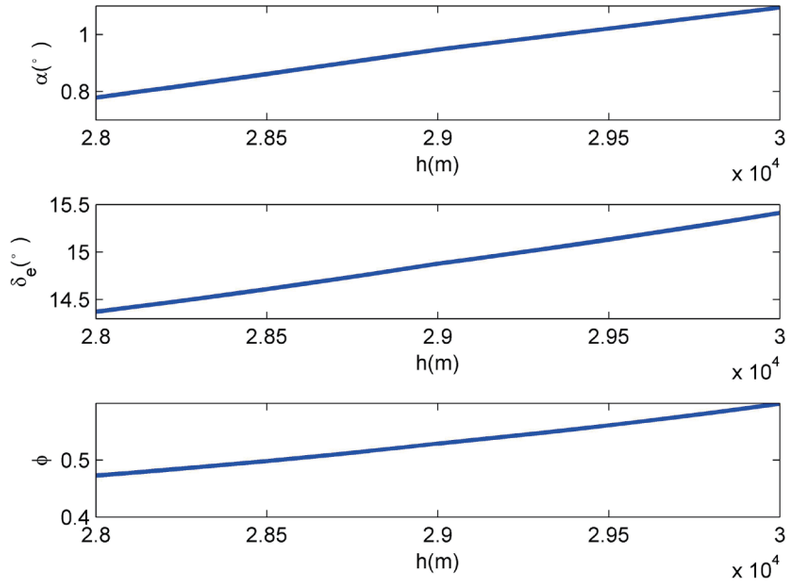

Fig.6. Trim states in consideration of static feature specification

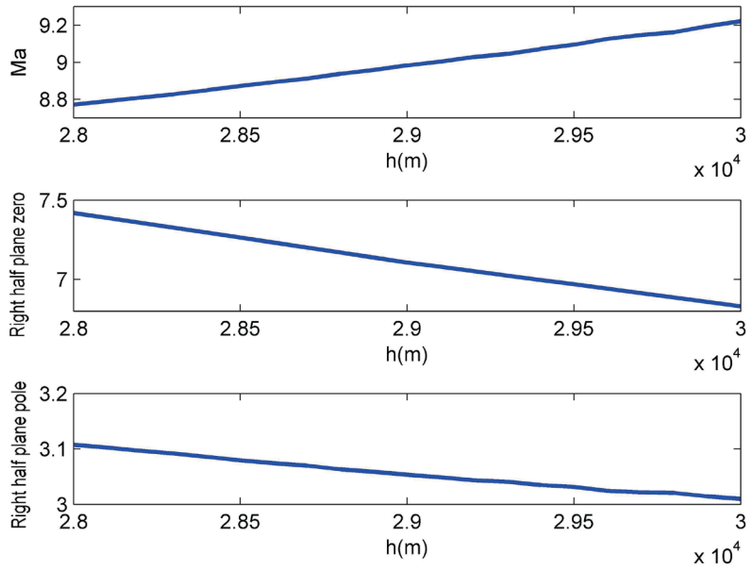

Fig.7. Optimal results in consideration of dynamic characteristic specification

performance indices. Nevertheless, the feasibility of the proposed method is important in the conceptual design stage for hypersonic vehicles.

5. Conclusion

A compromise optimal design strategy for hypersonic vehicles is presented. The dynamic model is established using multidisciplinary knowledge to analyze the static and dynamic features. Performance specifications are determined from the integrated design viewpoint, and the optimization method is discussed to obtain the optimum flight condition. Furthermore, a simulation example is provided to test the feasibility of the proposed approach. The resulting curves show that the compromise performance indices associated with static features and dynamic characteristics are suitable for the integrated design of

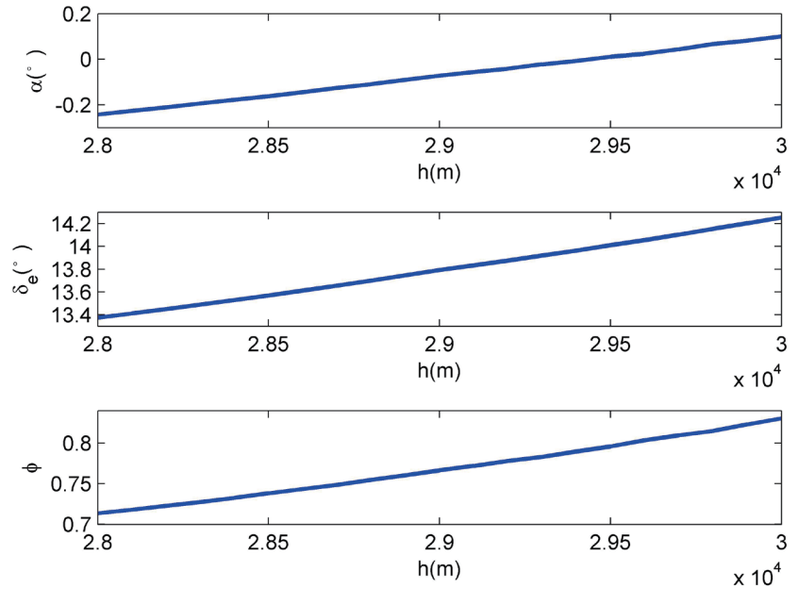

Fig.8. Trim states in consideration of dynamic characteristic specification

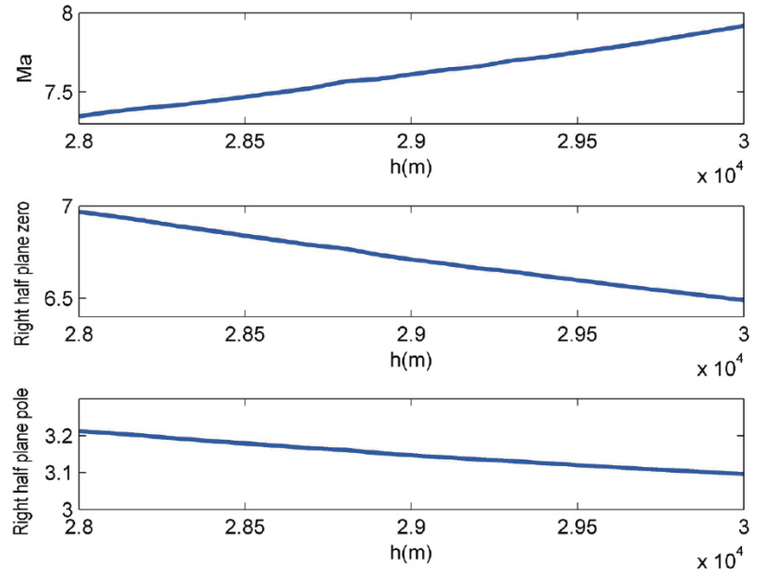

Fig.9. Optimal results in consideration of compromise optimal specification

DOI: http://dx.doi.org/10.5139/IJASS.2015.16.2.137

hypersonic vehicles. This work is beneficial for future studies on the design of a complex three-dimensional waverider configuration by using multidisciplinary optimization for hypersonic vehicles.

Acknowledgement

The authors thank the editors and the reviewers for their help and improvements to the quality of our presentation. This work is supported by National Natural Science Foundation of China under Grant No. 61403191; Beijing University of Aeronautics and Astronautics Open Funding Project of State Key Laboratory of Virtual Reality Technology and Systems under Grant No. BUAA-VR-14KF-03 and No. BUAA-VR-14KF-06.

References

[1] Kelkar, A. G., Vogel, J. M. and Inger, G., et al., "Modeling and Analysis Framework for Early Stage Trade-off Studies for Scramjet-Powered Hypersonic Vehicles", *Proceedings of the 16th AIAA/DLR/DGLR International Space Planes and Hypersonic Systems and Technologies Conference*, Norfolk, Virginia, 2009.

[2] Soloway D, I., Ouzts, P. J. and Wolpert, D. H., et al., "The Role of Guidance, Navigation, and Control in Hypersonic

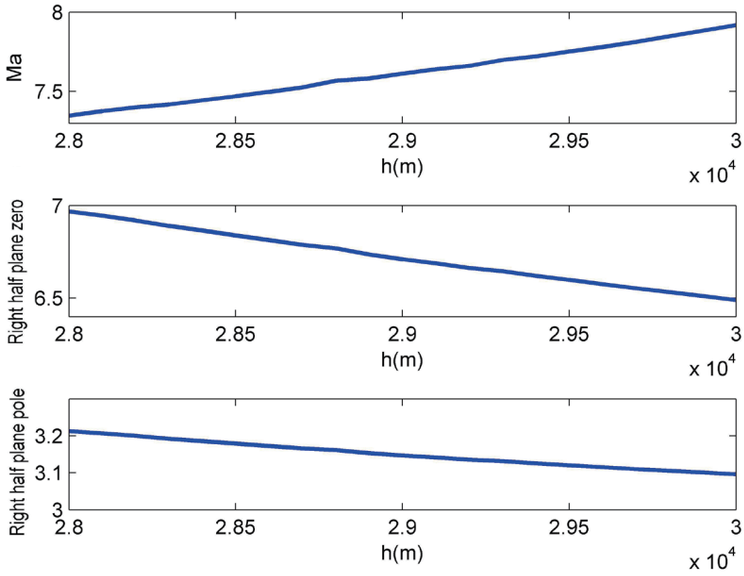

Fig.10. Trim states in consideration of compromise optimal specification

Table 2. Comparable results regarding different specifications

Selected specifications	Altitude (*km*)	Mach	Trim angle of attack (deg)	Right half plane zero	Trim elevator angle (deg)	Trim equivalence ratio
Static feature in Equation (12)	28	6.92	0.78	6.72	14.37	0.47
	30	7.51	1.09	6.29	15.41	0.60
Dynamic feature in Equation (15)	28	8.77	-0.24	7.42	13.37	0.71
	30	9.22	0.10	6.83	14.25	0.83
Integrated index in Equation (16)	28	7.35	0.51	6.97	13.98	0.52
	30	7.92	0.83	6.49	15.00	0.65

Vehicle Multidisciplinary Design and Optimization", *Proceedings of the 16th AIAA/DLR/DGLR International Space Planes and Hypersonic Systems and Technologies Conference*; , Norfolk, Virginia, 2009.

[3] Whitmer C., Kelkar, A. G. and Vogel, J. M., et al., "Control Centric Parametric Trade Studies for Scramjet-Powered Hypersonic Vehicles", *Proceedings of the 2010 AIAA Guidance, Navigation, and Control Conference*, Toronto, Ontario Canada, 2010.

[4] Park, C., "Hypersonic Aerothermodynamics: Past, Present and Future", *International Journal of Aeronautical and Space Sciences*, Vol. 14, No. 1, 2013, pp. 1-10.

DOI: 10.5139/IJASS.2013.14.1.1

[5] Bolender, M. A. and Doma, D. B., "Nonlinear Longitudinal Dynamical Model of an Air-Breathing Hypersonic Vehicle", *Journal of Spacecraft and Rockets*, Vol. 44, No. 2, 2007, pp 374-387.

DOI: 10.2514/1.23370

[6] Parker, J.K., Serrani, A. and Yurkovich, S., et al., "Control-Oriented Modeling of an Air-Breathing Hypersonic Vehicle", *Journal of Guidance, Control, and Dynamics*, Vol. 30, No. 3, 2007, pp. 856-869. DOI: 10.2514/1.27830

[7] Zeng, K. C., Xiang, J. W. and Li, D.C., "Aeroservoelastic modeling and analysis of a canard-configured air-breathing hypersonic vehicles", *Chinese Journal of Aeronautics*, Vol. 26, No. 4, 2013, pp. 831-840.

DOI: 10.1016/j.cja.2013.06.001

[8] Colgren, R., Keshmiri, S. and Mirmirani, M., "Nonlinear Ten-Degree-of-Freedom Dynamics Model of a Generic Hypersonic Vehicle", *Journal of Aircraft*, Vol. 46, No. 3, 2009, pp. 800-813.

DOI: 10.2514/1.35644

[9] Frendreis, S. V., and Cesnik, C. E., "3D Simulation of Flexible Hypersonic Vehicles", *Proceedings of AIAA Atmospheric Flight Mechanics Conference*, Toronto, Ontario Canada, 2010.

[10] Gao, G. and Wang, J. Z., "Reference command tracking control for an air-breathing hypersonic vehicle with parametric uncertainties", *Journal of the Franklin Institute-Engineering and Applied Mathematics*, Vol. 350, No. 5, 2013, pp. 1155-1188.

DOI: 10.1016/j.jfranklin.2013.02.012

[11] Huang, Y. Q., Sun, C. Y. and Qian, C. S., et al., "Non-fragile switching tracking control for a flexible air-breathing hypersonic vehicle based on polytopic LPV model", *Chinese Journal of Aeronautics*, Vol. 26, No. 4, 2013, pp. 948-959.

DOI: 10.1016/j.cja.2013.04.036

[12] Sun, H. B., Li, S. H. and Sun, C.Y., "Finite time integral sliding mode control of hypersonic vehicles", *Nonlinear Dynamics*, Vol. 73, No. 1, 2013, pp. 229-244.

DOI: 10.1007/s11071-013-0780-4

[13] Zong, Q., Wang, J. and Tao, Y., "Adaptive high-order dynamic sliding mode control for a flexible air-breathing hypersonic vehicle", *International Journal of Robust and Nonlinear Control*, Vol. 23, No. 15, 2013, pp. 1718-1736.

DOI: 10.1002/rnc.3040

[14] Xu, B., Shi, Z. K. and Yang, C. G., et al., "Neural control of hypersonic flight vehicle model via time-scale decomposition with throttle setting constraint", *Nonlinear Dynamics*, Vol. 73, No. 3, 2013, pp. 1849-1861.

DOI: 10.1007/s11071-013-0908-6

[15] Qi, R.Y., Huang, Y. H. and Jiang, B., et al., "Adaptive backstepping control for a hypersonic vehicle with uncertain parameters and actuator faults", *Proceedings of the Institution of Mechanical Engineers Part I-Journal of Systems and Control Engineering*, Vol. 227, No. 11, 2013, pp. 51-61.

DOI: 10.1177/0959651812450134

[16] Dalle, D.J., Torrez, S. M. and Driscoll, J. F., "Sensitivity of Flight Dynamics of Hypersonic Vehicles to Design Parameters", *Proceedings of 18th AIAA/3AF International Space Planes and Hypersonic Systems and Technologies Conference*, Tours, France, 2012

[17] Sridharan, S. and Rodriguez, A. A., "Impact of Control Specifications on Vehicle Design for Scramjet-Powered Hypersonic Vehicles", *Proceedings of AIAA Guidance, Navigation, and Control (GNC) Conference*, Boston, MA. 2013.

[18] Sridharan, S. and Rodriguez, A. A., "Performance Based Control-Relevant Design for Scramjet-Powered Hypersonic Vehicle", *Proceedings of AIAA Guidance, Navigation, and Control Conference*, Minneapolis, Minnesota, 2012.

[19] Tsuchiya, T., Takenaka, Y. and Taguchi, H., "Multidisciplinary Design Optimization for Hypersonic Experimental Vehicle", *AIAA Journal*, Vol. 45, No. 7, 2007, pp. 1655-1662.

DOI: 10.2514/1.26668

[20] Kelkar A. G., Vogel, J. and Whitmer. C., et al., "Design Tool for Control-Centric Modeling, Analysis, and Trade Studies for Hypersonic Vehicles", *Proceedings of 17th AIAA International Space Planes and Hypersonic Systems and Technologies Conference*, San Francisco, California, 2011.

[21] Starkey, R. P. and Lewis, M. J., "A shock-expansion method for determining surface properties on irregular geometries", *Proceedings of 40th Aerospace Sciences Meeting & Exhibit*, Reno, Nevada, 2002.

[22] Torrez, S. M., Driscoll, J. F. and Bolender, M. A., et al, "Effects of Improved Propulsion Modelling on the Flight Dynamics of Hypersonic Vehicles", *Proceedings of AIAA Atmospheric Flight Mechanics Conference and Exhibit*, Honolulu, Hawaii. 2008.

[23] Rodriguez, A. A., Dickeson, J. J. and Cifdaloz, O., et al, "Modeling and Control of Scramjet-Powered Hypersonic Vehicles: Challenges, Trends, and Tradeoffs", *Proceedings of AIAA Guidance, Navigation and Control Conference and Exhibit*, Honolulu, Hawaii. 2008.

[24] Clark, A., Wu, C. and Mirmirani, M., et al., "Development of an Airframe-Propulsion Integrated Generic Hypersonic Vehicle Model", *Proceedings of 44th AIAA Aerospace Sciences Meeting and Exhibit*, Reno, Nevada. 2006.

[25] Dickeson, J.J., Rodriguez, A, A. and Sridharan, S., et al., "Elevator Sizing, Placement, and Control-Relevant Tradeoffs for Hypersonic Vehicles", *Proceedings of AIAA Guidance, Navigation, and Control Conference*, Toronto, Ontario Canada. 2010.

[26] Liu, Y. B. and Lu, Y. P., "Conceptual research on modelling and control integrative design methods for hypersonic waverider", *Proceedings of the Institution of Mechanical Engineers Part G-Journal of Aerospace Engineering*, Vol. 225, No. 12, 2011, 1291-1301.

[27] Sachs, G. and Moravszki, C., "Predictive Tunnel Display for Hypersonic Flight Path Control", *Proceedings of AIAA Guidance, Navigation, and Control Conference and Exhibit*, Keystone, Colorado. 2006.

[28] Bolender, M. A. and Doma, D. B., "Flight Path Angle Dynamics of Air-breathing Hypersonic Vehicles", *Proceedings of AIAA Guidance, Navigation, and Control Conference and Exhibit*, Keystone, Colorado, 2006.